

Fast 3D Near-Infrared Breast Imaging Using Indocyanine Green for Detection and Characterization of Breast Lesions

Schnelle 3-D-Nah-Infrarot-Bildgebung der Brust unter Verwendung von Indocyaningrün für die Detektion und Charakterisierung von Läsionen in der weiblichen Brust

Autoren

P. Schneider¹, S. Piper², C. H. Schmitz^{2,7}, N. F. Schreiter^{1,3}, N. Volkwein¹, L. Lüdemann⁴, U. Malzahn⁵, A. Poellinger¹

Institute

Affiliation addresses are listed at the end of the article.

Key words

- breast
- laser
- contrast agents
- technical aspects

Zusammenfassung



Ziel: Evaluierung eines schnellen 3-D-Nah-Infrarot-Bildgebungsverfahrens unter Verwendung von Indocyaningrün (ICG) für die Detektion und Charakterisierung von Brustläsionen.

Material und Methoden: 30 Patientinnen mit mammografisch und/oder sonografisch detektierten suspekten Brustläsionen wurden mit einem schnellen optischen 2 Hz 3-D-Mammografen vor, während und nach Gabe eines 25 mg ICG-Bolus vor histologischer Sicherung mittels Stanzbiopsie untersucht. Die Boluskinetik wurde mithilfe von zwei Perfusionsparametern und einem abgeleiteten Parameter analysiert: „peak amplitude“ (PA), „time to peak“ (TTP) und „peak-time grouped amplitude“ (PTA). Mithilfe einer Receiver-operating-characteristic(ROC)-Analyse wurde ein PTA-Cut-off-Wert für eine untersucherunabhängige Differenzierung zwischen benignen und malignen Läsionen festgelegt. Acht Patientinnen mussten von der Datenauswertung ausgeschlossen werden. Insgesamt wurden 14 Brüste mit malignen Läsionen, 8 Brüste mit benignen Läsionen und drei gesunde Brüste analysiert.

Ergebnisse: Die cut-off-basierte PTA-Analyse führte zur korrekten Detektion bei 12 von 14 malignen Läsionen (Tumorgröße 8 – 80 mm; Sensitivität = 85,7%). Zwei maligne Läsionen wurden nicht erkannt. In der benignen Studiengruppe wurde lediglich ein Fibroadenom detektiert (Spezifität = 87,5%). PTA-Werte unterschieden sich signifikant für benigne und maligne Studiengruppe (Mann-Whitney U Test, $p < 0,05$). Brüste mit malignen Läsionen zeigten höhere Peaks zu früheren Zeitpunkten in der ICG-Perfusion.

Schlussfolgerung: Die frühe Perfusionsanalyse in der ICG-gestützten optischen 3-D-Mammografie konnte unterschiedliche Muster der Kontrastmitteleaufnahme in benignen und malignen Läsionen aufzeigen. Dieser Ansatz könnte der Detektion maligner Brustläsionen und der Abgrenzung zu benignen Herden dienen.

Abstract



Purpose: To evaluate fast 3D near-infrared breast imaging using the optical contrast agent indocyanine green (ICG) for the detection and characterization of breast lesions.

Materials and Methods: 30 patients with suspicious breast lesions on mammography and/or ultrasound underwent fast 2 Hz 3D optical mammography before, during, and after administration of a 25 mg ICG bolus prior to needle biopsy. The bolus kinetics is analyzed using two perfusion parameters and a derived parameter: “peak amplitude” (PA), “time-to-peak” (TTP) and “peak-time grouped amplitude” (PTA). A receiver operating characteristic curve (ROC) analysis was performed to define a PTA cut-off for reader-independent differentiation of benign and malignant lesions. 8 patients had to be excluded from data analysis. Overall 14 breasts bearing a malignant lesion, 8 breasts bearing a benign lesion and 3 healthy breasts were analyzed.

Results: The cut-off-based PTA analysis allowed correct detection for 12 of 14 malignant lesions (tumor size: 8 – 80 mm; sensitivity = 85.7%). Two malignant lesions were missed. In the benign study group only one fibroadenoma was detected (specificity = 87.5%). The PTA values differed significantly between the benign group and the malignant group (Mann-Whitney U-test, $p < 0.05$). Breasts with malignant lesions showed higher peaks at early time-points in ICG perfusion.

Conclusion: Early perfusion analysis of ICG-enhanced 3D fast optical mammography revealed different enhancement patterns for benign and malignant lesions. This approach might help with the detection of malignant breast lesions and the differentiation from benign lesions.

eingereicht 13.6.2011

akzeptiert 2.8.2011

Bibliografie

DOI <http://dx.doi.org/10.1055/s-0031-1281726>

Online-Publikation: 2011
Fortschr Röntgenstr 2011; 183: 956–963 © Georg Thieme Verlag KG Stuttgart · New York · ISSN 1438-9029

Korrespondenzadresse

Dr. Alexander Poellinger

Radiology, Charité,
Campus Mitte
Schumannstr. 20/21
10117 Berlin
Germany
Tel.: ++49/30/4 50 62 72 69
Fax: ++49/30/4 50 52 79 09
alexander.poellinger@charite.de

Introduction

Near-infrared (NIR) diffuse optical imaging is one of several new techniques that are currently under development for the detection and characterization of breast lesions [1–8]. While established modalities such as mammography and ultrasound mainly rely on morphological information, optical imaging has the potential to provide information on the molecular and cellular level that may improve the detection and characterization of tumorous tissue [9, 10]. In recent years, most approaches were based on the intrinsic tissue contrast of hemoglobin, water, and lipids [11–13]. In particular, the increased hemoglobin content of malignancies due to neoangiogenesis was expected to result in marked contrast between malignant lesions and surrounding breast tissue. However, NIR scans using endogenous contrast often also display lesions with increased vascularization other than cancer, such as fibroadenomas, fibrocystic changes or simply dense glandular tissue [14, 15]. As a result, it is difficult to differentiate such regions from malignant lesions when no additional information is available. One possible way to overcome these limitations might be the use of contrast agents that enhance the contrast between carcinomatous and non-diseased breast tissue. Optical contrast agents may increase light absorption and emission of fluorescence, for example. In recent years, a few pilot breast imaging studies have been performed using indocyanine green (ICG), a weakly fluorescent dye [16–18]. ICG is a water-soluble tricarboxyanine dye introduced in 1957 by Fox et al. [19]. The compound is very safe and is approved by the U.S. Food and Drug Administration [20]. It exhibits an absorption and fluorescence spectrum in the near-infrared window [21]. ICG is considered a blood pool agent because of its high binding affinity to serum proteins like albumin, α -1-lipoproteins and β -1-lipoproteins [22] that cannot pass through the endothelium of normal vessels. During early enhancement, tissue concentration contrast is mainly determined by intravascular contributions [23]. Few recent studies have aimed at exploiting spatiotemporal features of ICG distribution in the diseased breast, notably one study on late-fluorescence of ICG [23] and another using pharmacokinetic-rate images based on absorption of ICG [24]. The aim of our study was to assess fast (2 Hz) 3D dynamic optical imaging for the detection of breast cancer and the differentiation between benign and malignant breast lesions.

Materials and Methods

Patients

The ethical review board of BLINDED approved this study. All patients provided written informed consent. From December 2008 to November 2009, 30 consecutive women (age: 29 to 77 years, median 51 years) with 30 suspicious breast lesions (=target lesions) referred for biopsy were examined in our study. Before biopsy all patients underwent ultrasound, 29 patients received X-ray mammography and 25 patients obtained dynamic contrast-enhanced magnetic resonance imaging (DCE-MRI). DCE-MRI was performed at 1.5 T (Signa Twin-Speed, General Electric Medical Systems, Milwaukee) using a T1-weighted fat-suppressed sequence (TR=6.4 msec, TE=2.1 msec, flip angle: 10°, matrix 256×160, effective slice thickness: 1.5 mm). The inclusion criteria were suspicious breast lesions detected by X-ray mammography or ultrasound (Breast

Imaging Reporting and Data System (BI-RADS) scores of 4 and 5). The exclusion criteria were age under 18 years, breast size greater than 34B (US system), needle biopsy or surgery of the ipsilateral breast within the previous 6 months, ulcers or wounds of the ipsilateral breast, and known anaphylactic reaction. Further exclusion criteria were abnormal levels of aspartate aminotransferase, gamma glutamyl transferase, creatinine and thyroid stimulating hormone. 8 of the 30 patients were excluded from data analysis: 5 patients due to high noise in the raw data probably caused by insufficient coupling of the interface and the breast (a problem that occurred in the first patients and was later resolved). Another patient was excluded because of her large breast size, which exceeded the breast cup of the optical imager, 2 more patients because of different histological findings (melanoma metastasis, T-cell lymphoma). The final data analysis comprised 22 patients (25 breasts): 14 patients with 1 malignant lesion each (median age 60 years, range 31 to 77 years) and 8 patients with 8 benign lesions (median age 32 years, range 27 to 50 years). In addition, there was a control group of three breasts without any lesions (as verified by MRI and by 1.5 years follow-up): two contralateral breasts of two patients of the benign group and one contralateral breast of the malignant group.

For all women breast density was classified by an experienced radiologist using the standard BI-RADS scale: 1=almost completely fat, 2=scattered fibroglandular densities, 3=heterogeneously dense, and 4=extremely dense. Results were dichotomized between the two densest and two least dense BI-RADS categories into “nondense” and “dense breasts”.

NIR Imaging

Breast examination was performed using a DYNOT 232 optical tomography system (NIRx Medical Technologies LLC, NY, USA) customized for mammography studies. The device is CE marked. 31 fiber optic sensors, each containing an optical source and detector, were placed in contact with the breast by means of a rigid plastic cup. Different breast sizes were accommodated by varying the protrusion of the fibers into the cup. A detailed description of the system is given in [25]. The fiber holder was mounted on a gantry positioned under a modified patient bed. The gantry slides sideways to be used on either breast and can be height-adjusted to bring the cup up against the patient's chest wall through an opening in the bed. The women remained in the prone position throughout the examination. The instrument performs sequential illumination at each fiber position while simultaneously acquiring detector readings for each illumination site, resulting in a total of 961 measurements at a rate of approx. 2 Hz. The scanner performs simultaneous dual-wavelength measurements at 760 nm and 830 nm.

All imaging was performed prior to biopsy. Optical scanning was carried out over a total scanning time of 25 min and comprised two steps: a 5 min scan before and a 20 min scan during and after bolus administration of 25 mg ICG (PULSION Medical Systems AG, Munich, Germany) diluted in 15 ml aqua ad injectionem (injection time: 5 sec). The ICG bolus was followed by a 15 ml saline flush.

Pathology

Tissue of target lesions obtained by vacuum-assisted core needle biopsy (n=14) or surgical excision (n=16) were used for histopathological examination by the local pathology department. In

the final analysis group of 22 patients, diameters for 10 of the 14 malignant lesions were determined by histopathology, MRI was used for 4 lesions. In the benign group the diameters of 5 lesions were measured by MRI and 3 by ultrasound.

Data Analysis

Data Preprocessing and Reconstruction

After data acquisition optical raw data were preprocessed with NIRx NAVI software (Near Infrared Analysis, Visualization and Imaging, Rev. 8.11 by NIRx), a program based on Matlab 6.5 software (The Mathworks, Inc., Natick, MA). Data were low-pass-filtered ($f_{\text{cutoff}} \approx 0.075$ Hz) to suppress heart beat, higher-frequency noise, and motion artifacts. Channels which exhibited excessive noise (coefficient of variation (C.V.) > 25%) during the rest phase were excluded. All included data channels were normalized with respect to the temporal mean value during rest. From the preprocessed data we reconstructed 3D time series of relative ICG concentration changes over a total of 2243 volume segments. Time series images were reconstructed with the normalized-difference method using a precomputed weight function that was generated using a finite element method (FEM) solver of the diffusion equation [26].

Data reconstruction was based on the measurement of the 760 nm wavelength since absorption properties of ICG over different ICG concentrations in plasma are rather constant at this wavelength as opposed to the 830 nm wavelength [27]. Data analysis was performed using customized routines in Matlab.

Definition of Perfusion-Based Parameters

To evaluate differences in contrast dynamics for various breast lesions, two common perfusion parameters in the image time series were measured: peak amplitude (PA) and time-to-peak (TTP). PA was defined as the maximum amplitude for each time course per voxel and was normalized to the mean amplitude of the entire breast volume. TTP was defined as the time between the earliest time-point (t_0) at which more than 0.25% (value derived by optimizing analysis) of the breast volume exhibited a peak in intensity and the time-point of PA for each voxel. These perfusion-based parameters were selected, as they proved particularly robust across experiments.

To reveal differences between breasts bearing malignant or benign lesions, we performed an analysis based on the TTP and PA values. A 15 sec interval (30 time-points) following the above-defined TTP reference time-point t_0 was selected. For

each of these 30 time-points the amplitudes of all voxels across all benign or malignant cases reaching the maximum were averaged for the benign and malignant group separately (PTA, peak time-grouped amplitudes). The result was visualized in a PA vs. TTP curve (PTA curve). This numerical approach focuses on temporal information of ICG perfusion in the whole breast without providing any information on the spatial distribution of lesions.

ROC Analysis and Statistical Analysis

Derivation of the PTA parameter allowed the use of standard statistical tests to evaluate its diagnostic power. Based on the two separate PTA curves for the benign and malignant group, the standardized mean difference (SMD) between these groups at each time-point was computed. SMD is defined as the difference of the means for two different groups divided by the pooled standard deviation and is commonly used in practical meta-analysis. Specifically, the following definition was used:

$$\text{SMD} = \frac{\bar{X}_{\text{malignant}} - \bar{X}_{\text{benign}}}{\sqrt{\frac{1}{(n_1 + n_2 - 2)}((n_1 - 1) \cdot \text{Var}(X_{\text{malignant}}) + (n_2 - 1) \cdot \text{Var}(X_{\text{benign}}))}}$$

with $X_{\text{malignant}}$ and X_{benign} being the mean amplitudes of the malignant and the benign group and n_1 , n_2 number of breasts in the malignant and benign group, respectively.

The greatest difference in ICG absorption between the two groups is reached when SMD is at the maximum.

A Mann-Whitney U-test was applied to compare the distributions of amplitudes between the malignant and the benign group or the healthy control group. A p-value of <0.05 was considered significant. Finally, a receiver operation characteristic (ROC) analysis was conducted at the time-point of maximum SMD, and the sensitivity and specificity were derived. Data of the control group were not included in the ROC analysis.

Results



The histological findings and lesion dimensions are summarized in **Table 1**. There were 11 radiolucent breasts (10 malignant lesions, 1 benign lesion) and 10 radiodense breasts (4 malignant lesions, 6 benign lesions). For one breast no mammography was available. All breasts in the control group were radiodense.

Table 1 Histopathological findings.¹

Tab. 1 Histologische Ergebnisse.

histopathologic Result	no. of Lesions	mean lesion size/range (mm) ²	detection with NIR	correct location with NIR
benign (n = 8)	8		1/8	1/8
fibroadenoma	6	24 mm (10 – 52 mm)	1/6	1/6
mastopathy	1	11 mm	0/1	0/1
pseudoangiomatous stromal hyperplasia	1	44 mm	0/1	0/1
malignant (n = 14)	14		12/14	12/14
invasive ductal carcinoma	9	29 mm (8 – 51 mm)	8/9	8/9
invasive lobular carcinoma	1	25 mm	1/1	1/1
invasive lobular ductal carcinoma	1	17 mm	0/1	0/1
ductal carcinoma in situ	1	80 mm	1/1	1/1
metaplastic carcinoma	2	28 mm (19 – 37 mm)	2/2	2/2

¹ N/A: not applicable.

² Mean lesion size, with size range in parentheses, is given in cases of more than one lesion.

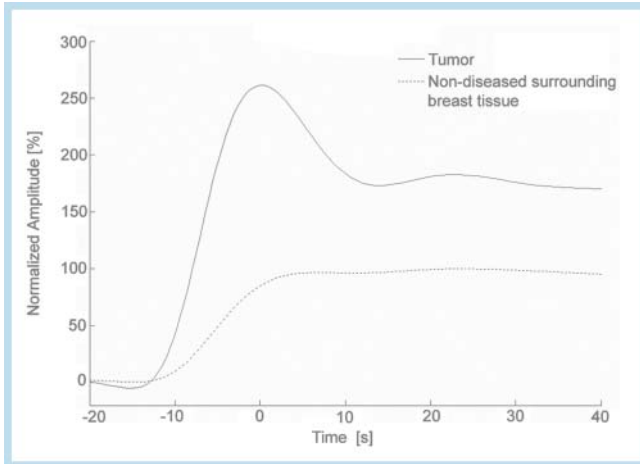


Fig. 1 Case of a 77-year-old patient bearing a 19-mm metaplastic carcinoma in her left breast. Highly temporally resolved (2 Hz acquisition rate) time/intensity curves of the malignant tumor (solid line) and of the non-diseased surrounding breast tissue (solid dotted line). Curves were normalized to maximum of non-diseased tissue curve.

Abb. 1 77-jährige Patientin mit einem 19-mm metaplastischen Karzinom in der linken Brust. Zeitlich hochaufgelöste (2 Hz Akquisitionsrate) Zeitintensitätskurven des malignen Tumors (durchgezogene Linie) und des umgebenden tumorfreien Brustgewebes (gestrichelte Linie). Die Kurven wurden auf das Kurvenmaximum des tumorfreien Brustgewebes normalisiert.

A representative ICG bolus response in the reconstructed time series data is shown in **Fig. 1** for a 77-year-old woman bearing a 19 mm carcinoma in her left breast. Two spatially averaged response curves are displayed, one from an area in the presumed tumor region, and another measured in the non-diseased pe-

riphery. This example illustrates the marked perfusion differences between both tissues, i.e. early enhancement in the malignant lesion and prolonged enhancement in the surrounding tissue.

Time-to-Peak-Based Amplitude Analysis

Fig. 2 summarizes the results of the PTA analysis. **Fig. 2a** shows the PA vs. TTP plot for both the malignant and the benign group. For the first 4–5 seconds from t=0 sec, the median amplitudes of the malignant group are bigger than those of the benign group leading to high values of the standardized mean difference (SMD). After 5 seconds a rather constant plateau can be discerned for the malignant group while for the benign group a further increase in amplitude (median amplitude = 122.6%) up to 12.5 sec can be observed. The best discriminatory power between the malignant and benign group is expected when the standardized mean difference is at the maximum. In our study, we observed the maximum SMD after 1.5 sec (SMD = 1.76) when the median of peak amplitude reached 55.8% (min 9.8%, max 99.6%) for the benign group and 111.0% (min 30.4%, max 187.0%) for the malignant group (**Fig. 2b**). The Mann-Whitney U-test yields a significant difference in peak amplitudes between the two groups (p = 0.0015). At the time-point of 1.5 sec, we performed an ROC analysis (**Fig. 2c**). Using a cut-off point at 84.4% of amplitude, a sensitivity of 85.7% and a specificity of 87.5% were achieved. 7 of 8 breasts bearing benign lesions showed amplitudes below this cut-off point, while 12 of 14 breasts with malignant lesions exhibited amplitudes of more than 84.4%. The highest amplitude (187.0%) was observed for a breast bearing a 33-mm IDC in a 53-year-old patient (case I, **Fig. 3**). The two cases that showed low amplitudes were a moderately graded IDC with a diameter of 15-mm in a 55-year-old patient (amplitude: 30.4%) and a mixed invasive lobu-

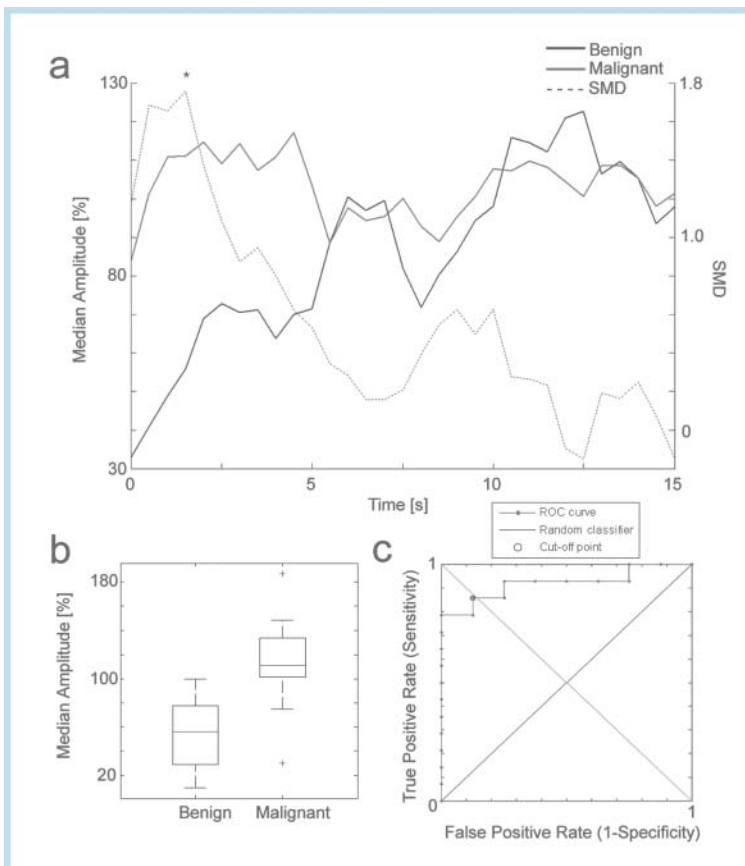


Fig. 2 Time-to-peak-based amplitude analysis for 22 patients. **a** Analysis of peak amplitudes for a time interval of 15 seconds after the appearance of first ICG bolus peaks in the breast (t = 0 sec). At each time-point the median of averaged amplitudes of all examined breasts was plotted for benign (solid black) and malignant (solid gray) lesions. The standardized mean difference (SMD) for each time-point is indicated by the dotted line; the asterisk (*) marks the maximum SMD at t = 1.5 sec. **b** Box plots illustrate peak amplitudes at 1.5 sec for both groups; center lines mark the median, center box edges envelope the upper and lower quartile, whiskers represent the lowest data still within the 1.5 interquartile range (IQR) of the lower quartile and the highest data still within the 1.5 IQR of the upper quartile. Outliers are represented by crosses. **c** ROC curve for peak amplitudes at 1.5 sec. The cut-off point was set to 84.4%.

Abb. 2 Time-to-peak basierte Amplitudenanalyse für 22 Patientinnen. **a** Analyse der Peakamplituden für ein Zeitintervall von 15 sec. nach Auftreten der ersten ICG-Bolus Peaks in der Brust (t = 0 sec.). Für jeden Zeitpunkt wurde der Median der gemittelten Amplituden aller untersuchten Brüste mit benignen (durchgezogen schwarz) und malignen (durchgezogen grau) Läsionen dargestellt. Die standardisierte Mittelwertsdifferenz (SMD) beider Gruppen wird für jeden Zeitpunkt angegeben (gestrichelte Linie); der Stern (*) markiert die maximale SMD bei t = 1,5 sec. **b** Boxplots zur Illustration der Verteilung der Peakamplituden bei t = 1,5 sek für beide Gruppen; Mittellinien repräsentieren den Median; Boxecken umschließen das obere und untere Quartil; Whisker repräsentieren die niedrigsten bzw. höchsten Datenwerte jeweils begrenzt auf 1,5 Interquartilsabstand (IQR) des unteren bzw. oberen Quartils. Ausreißer werden durch Kreuze dargestellt. **c** ROC Kurve für Peakamplituden bei t = 1,5 sec. Der Cut-Off-Wert wurde auf 84,4% gesetzt.

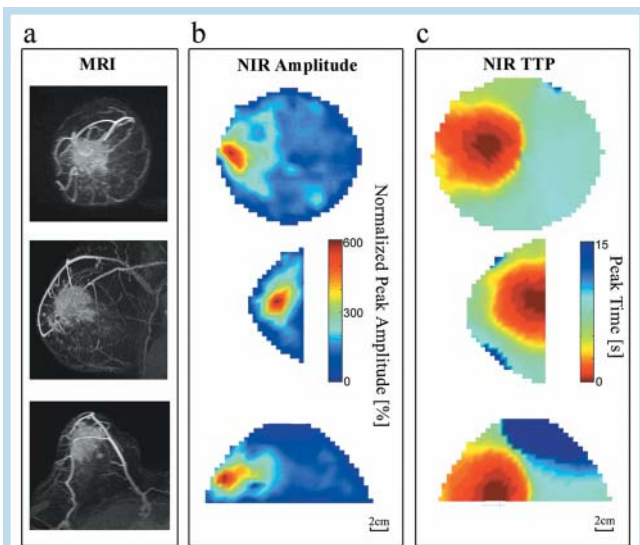


Fig. 3 Magnetic resonance mammography shows a large area of hypervascularization at the 9 o'clock position **a** corresponding with higher amplitudes in this area in the "peak amplitude map" **b** and earlier times in the "time-to-peak map" **c** in indocyanine-enhanced NIR imaging. Histology revealed a 33-mm intermediate grade IDC in a 53-year-old woman.

Abb. 3 Die Magnetresonanz Mammographie zeigt ein großes hypervaskularisiertes Areal in der 9 Uhr Position **a** korrespondierend mit höheren Amplituden in diesem Bereich in der „Peakamplituden Map“ **b** und früheren Zeitpunkten in der „time-to-peak Map“ **c** in der NIR Bildgebung mit Indocyaningrün. Die Histologie ergab ein 33-mm IDC intermediären Grades bei der 53-jährigen Patientin.

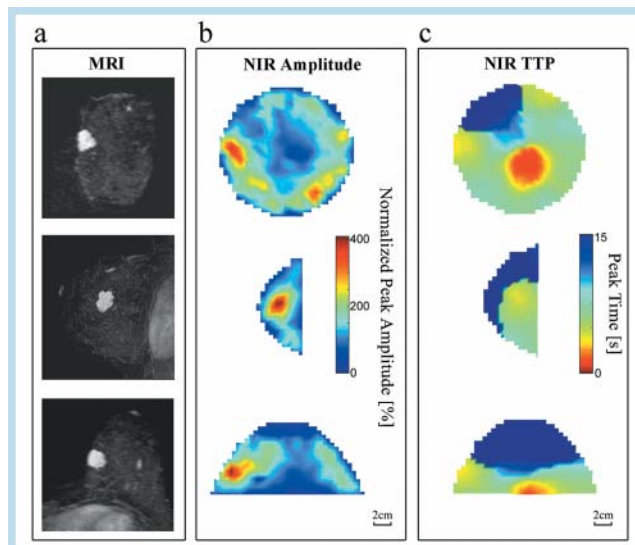


Fig. 5 22-mm fibroadenoma in a 27-year-old woman. **a** Gadolinium-enhanced subtraction MRI of a suspicious lesion located at the 9 o'clock position in the left breast. The lesion was palpated at 9 o'clock position. **b** Mapping of peak amplitude based on indocyanine-enhanced NIR imaging. **c** Mapping of times-to-peak based on indocyanine-enhanced NIR imaging.

Abb. 5 22-mm Fibroadenom bei einer 27-jährigen Patientin. **a** Gadoliniumbasierte Subtraktions-MRT der suspekten Läsion mit Lokalisation auf 9 Uhr in der linken Brust. Die Läsion konnte auf 9 Uhr palpirt werden. Darstellung der Peakamplituden **b** und der Peakzeiten **c** in der NIR Bildgebung mit Indocyaningrün.

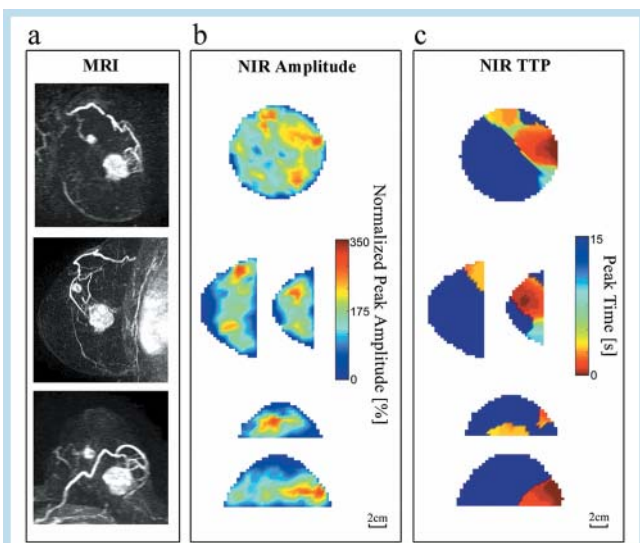


Fig. 4 Case of a 48-mm multicentric IDC in a 58-year-old woman. Gadolinium-enhanced subtraction MRI shows the suspicious lesions located at the 11 and 3 o'clock positions **a**. **b** Mapping of peak amplitude based on indocyanine-enhanced NIR imaging. **c** Mapping of times-to-peak based on indocyanine-enhanced NIR imaging.

Abb. 4 Fall eines 48-mm multizentrischen IDC bei einer 58-jährigen Patientin. Die gadoliniumbasierte MRT-Subtraktionsaufnahme zeigt die suspekten Läsionen mit Lokalisierung in der 11 und 3 Uhr Position **a**. Darstellung der Peakamplituden **b** und der Peakzeiten **c** in der NIR Bildgebung mit Indocyaningrün.

lar and ductal carcinoma (diameter: 16 mm) in a 61-year-old patient (amplitude: 74.7%). In the benign breast group there was only one case of a 10-mm FA in a 50-year-old woman with an amplitude of 99.6% leading to a false positive result. Regarding the healthy control group, all three breasts showed amplitudes below the cut-off point of 84.4% (median amplitude: 32.7%, min 22.5%, max 60.4%). Generally speaking, maximum intensities of the absorption signal at early peak times differed significantly between the malignant and the benign breast group. As a rule, breasts with malignant lesions showed high maxima at early time-points (▶ Fig. 3, 4) while there was a slow increase in amplitudes in early ICG-perfusion and high amplitudes appeared later in breasts bearing benign lesions (or without any lesion) (◀ Fig. 5).

Discussion

Using contrast-enhanced fast NIR imaging, we found significant differences in the enhancement kinetics of benign and malignant breast lesions. High temporal resolution analysis of the 3D dataset acquired before and after ICG administration depicted early peaks with high peak amplitudes in breasts bearing a malignant lesion. The combination of perfusion-derived parameters such as time-to-peak and peak amplitude distinguished the malignant group from the nonmalignant group with high accuracy (sensitivity=85.7%, specificity=87.5%, ppv=92.3%, npv=77.8%). It is important to note that these results were achieved without subjective evaluation by a reader but rather by a reader-independent analysis using

an amplitude cut-off identified by ROC analysis. The three healthy control breasts that were not included in the ROC analysis were also correctly classified as 'benign' using the defined cut-off value which separated the benign group from the malignant group.

An explanation for the rapid signal increase in breasts with malignant lesions might be the higher vessel density found in malignant tissue [28–30] as compared to that of non-malignant tissue. Our results are consistent with other studies using perfusion-derived imaging parameters: Alacam et al. investigated ICG pharmacokinetics using a two-compartment model [24] and also observed delayed enhancement in a fibroadenoma in comparison to malignancies. Although our study did not determine absolute perfusion values, our findings are in good agreement with these results.

It is well known from dynamic MRI that malignancies tend to show faster wash-in [6, 7, 31, 32] and earlier wash-out [2, 33]. However, most authors state that ultrafast data acquisition is not necessary for the detection of malignant lesions and a temporal resolution of ca. 1 minute is sufficient [34, 35]. On the contrary, some authors showed that by combining the results of ultrafast acquisition in MRI with those of the slow dynamic analysis improved the diagnostic performance significantly [36, 37].

In contrast to gadolinium-based contrast agents that exhibit fast and unspecific extravasation through capillaries, ICG shows different perfusion properties: As ICG binds to macromolecules like albumin, α -1-lipoproteins and β -1-lipoproteins [38], it acts as a macromolecular contrast agent with diagnostically useful dynamics on different timescales: (1) during early enhancement, tissue concentration contrast is determined by intravascular contributions [23], (2) in tumorous tissue, increased capillary permeability leads to extravasation of ICG. Recently, the feasibility of late fluorescence imaging based on extravasation of ICG for tumor detection and discrimination was demonstrated [39].

Generally speaking, the permeability of blood vessels for ICG is markedly smaller than for gadolinium-based contrast agents [23, 40]. We hypothesize that the different extravasation rate of ICG and gadolinium-based contrast agents is the major factor for the difference in early perfusion and is responsible for the early peaks observed in our study.

Moreover, studies using contrast-enhanced ultrasound observed a decrease in time-to-peak and a faster ascent of time intensity curves in malignant breast lesions [41–43]. Microbubble contrast agents are strictly confined to the vascular bed and thus should feature similar distribution as ICG in early perfusion.

There was one false positive finding in the benign group and two false negative findings in the malignant group indicating that there might be some overlap in perfusion characteristics between benign and malignant lesions in general. It is well known from other imaging modalities such as MRI that substantial overlap can exist in contrast enhancement properties for fibroadenomas and invasive breast cancers, so that lesion differentiation based only on the kinetic features can be difficult if not impossible [44].

In recent years, several studies using non-contrast-enhanced optical imaging were conducted. In a systematic review based on approximately 2000 optical mammographies, Leff et al. [45] concluded that only 85% of the lesions in general were detectable on the basis of their hemoglobin content. In particular,

small malignant lesions (<10 mm) as well as benign lesions such as fibroadenomas were difficult to identify. Moreover, intrinsic parameters were not capable of distinguishing benign lesions from malignancies. Even though a similar sensitivity was reached in our study, our technique seems to provide sufficient specificity by use of fast perfusion analysis following administration of an extrinsic dye.

Modern full field digital X-ray mammography has reached high quality standards in image quality [46] guaranteed by permanent evaluation [47–51]. Although continuous efforts to minimize radiation are undertaken [52, 53], X-ray mammography might cause double-strand breaks possibly leading to cell mutations. Recent studies show that X-ray mammography produced double-strand breaks in human mammary epithelial cells, exacerbated in women with a high family risk of breast cancer [54]. Due to the use of non-ionizing near-infrared light, optical tomography has a clear advantage over X-ray mammography in terms of ionizing radiation.

Major limitations of the study include the following: (a) the number of malignant and benign lesions was small. (b) There was a considerable median age difference between the malignant and benign group. Differences in breast perfusion might be caused by age-related differences in glandular density (involution) and perfusion parameters. (c) The analysis does not consider interindividual differences in blood circulation. Acquisition of the arterial input function (AIF) would be helpful to increase comparability. (d) The control group included only three breasts without any lesions. A larger number of controls would be useful to learn more about normal breast perfusion. (e) Finally the rather rigid design of the breast cup with insufficient adjustability for breasts too small or too big for the cup was the main reason for the high dropout rate in the study: In five breasts, sufficient contact between the optodes and the skin could not be established, resulting in poor data quality. One case of a rather big breast had to be discarded, as the dorsal areas of the breast were not covered. Similar limitations have been reported using other modalities like vacuum-assisted breast biopsy with the patient in the prone position [55]. Using an adjustable cup size could overcome this limitation.

In conclusion, our preliminary results show that early perfusion analysis of ICG-enhanced 3D optical mammography can help to detect malignant breast lesions and might make it possible to differentiate them from benign breast lesions. Using an ROC analysis, we achieved a sensitivity of 85.7% and a specificity of 87.5%. Assuming that improvements in scanner design will overcome some of the difficulties encountered in our study, this technique is promising and might serve as an adjunct method to X-ray mammography.

Acknowledgements

▼ This work was supported in part under NIH Grant Nos. R42NS050007 and R44NS049734. The authors would like to thank NIRx GmbH for providing the imaging equipment.

Institute

- ¹ Radiology, Charité Universitätsmedizin Berlin, Campus Virchow Klinikum
- ² Neurology, Berlin Neuroimaging Center (BNIC), Charité Universitätsmedizin Berlin
- ³ Klinik für Strahlenheilkunde, Charité Universitätsmedizin Berlin, Campus Virchow Klinikum
- ⁴ Department of Radiotherapy, Charité, Universitätsmedizin Berlin, Campus Virchow Klinikum
- ⁵ Center for Stroke Research Berlin (CSB), Charité Universitätsmedizin Berlin
- ⁶ Radiology, Charité Universitätsmedizin Berlin, Campus Mitte Klinikum
- ⁷ NIRx Medizintechnik GmbH, Berlin

References

- 1 Fischer U, Schwethelm L, Baum FT et al. Aufwand, Zuverlässigkeit und histologische Ergebnisse der MR-gesteuerten Vakuumbiopsie suspekter Mammabefunde – retrospektive Auswertung von 389 Interventionen. *Fortschr Röntgenstr* 2009; 181: 774–781
- 2 Baltzer PA, Dietzel M, Vag T et al. Können farbkodierte parametrische Karten die Analyse dynamischer Anreicherungsmuster in der MR-Mammografie verbessern? *Fortschr Röntgenstr* 2010; 182: 254–260
- 3 Müller-Schimpfle MP, Heindel W, Kettritz U et al. Konsensustreffen der Kursleiter in der Mammadiagnostik am 9.5.2009 in Frankfurt am Main – Thema: Herdbefunde. *Fortschr Röntgenstr* 2010; 182: 671–675
- 4 Adamietz B, Schulz-Wendtland R, Meier-Meitinger M. Asymptomatische Silikonome nach Prothesenruptur: Darstellung in der Elastografie. *Fortschr Röntgenstr* 2009; 181: 385–386
- 5 Meier-Meitinger M, Schulz-Wendtland R, Adamietz B. Brustmetastase – eine ungewöhnliche klinische Erstmanifestation eines primären Ovarialkarzinoms. *Fortschr Röntgenstr* 2009; 181: 1082–1084
- 6 Siegmann KC, Moron HU, Baur A et al. Diagnostische Wertigkeit des Göttinger Scores zur Malignitätsvorhersage von ausschließlich in der MRT darstellbaren Mammaläsionen. *Fortschr Röntgenstr* 2009; 181: 556–563
- 7 Siegmann KC, Müller KT, Vogel U et al. MR-Mammografie vor und nach neoadjuvanter Systemtherapie – Enhancementcharakteristika und T2-Signalintensität von Mammakarzinomen und Drüsenparenchym. *Fortschr Röntgenstr* 2010; 182: 493–500
- 8 Siegmann KC, Speck S, Baur A et al. Einsatz eines speziellen Clips (Tumark[®] Professional) zur postinterventionellen Markierung suspekter Mammaläsionen nach MRT-gestützter Vakuumbiopsie – erste Ergebnisse. *Fortschr Röntgenstr* 2009; 181: 147–154
- 9 Weissleder R, Pittet MJ. Imaging in the era of molecular oncology. *Nature* 2008; 452: 580–589
- 10 Tromberg BJ, Shah N, Lanning R et al. Non-invasive in vivo characterization of breast tumors using photon migration spectroscopy. *Neoplasia* 2000; 2: 26–40
- 11 Taroni P, Torricelli A, Spinelli L et al. Time-resolved optical mammography between 637 and 985 nm: clinical study on the detection and identification of breast lesions. *Phys Med Biol* 2005; 50: 2469–2488
- 12 Cerussi A, Shah N, Hsiang D et al. In vivo absorption, scattering, and physiologic properties of 58 malignant breast tumors determined by broadband diffuse optical spectroscopy. *J Biomed Opt* 2006; 11: 044005
- 13 Grosenick D, Moesta KT, Moller M et al. Time-domain scanning optical mammography: I. Recording and assessment of mammograms of 154 patients. *Phys Med Biol* 2005; 50: 2429–2449
- 14 Floery D, Helbich TH, Riedl CC et al. Characterization of benign and malignant breast lesions with computed tomography laser mammography (CTLM): initial experience. *Invest Radiol* 2005; 40: 328–335
- 15 Rinneberg H, Grosenick D, Moesta KT et al. Scanning time-domain optical mammography: detection and characterization of breast tumors in vivo. *Technol Cancer Res Treat* 2005; 4: 483–496
- 16 Ntziachristos V, Yodh AG, Schnall M et al. Concurrent MRI and diffuse optical tomography of breast after indocyanine green enhancement. *Proc Natl Acad Sci U S A* 2000; 97: 2767–2772
- 17 Intes X, Ripoll J, Chen Y et al. In vivo continuous-wave optical breast imaging enhanced with Indocyanine Green. *Med Phys* 2003; 30: 1039–1047
- 18 Azar FS, Lee K, Khamene A et al. Standardized platform for coregistration of nonconcurrent diffuse optical and magnetic resonance breast images obtained in different geometries. *J Biomed Opt* 2007; 12: 051902
- 19 Fox IJ, Brooker LGS, Haseltine DW et al. A tricarboyanine dye for continuous recording of dilution curves in whole blood independent of variations in blood oxygen saturation. *Proc Staff Meeting Mayo Clin* 1957; 32: 478–484
- 20 Jackson TL. Safety of indocyanine green as a vital stain. *Anesthesiology* 2004; 100: 1330
- 21 Desmettre T, Devoisselle JM, Mordon S. Fluorescence properties and metabolic features of indocyanine green (ICG) as related to angiography. *Surv Ophthalmol* 2000; 45: 15–27
- 22 Yoneya S, Saito T, Komatsu Y et al. Binding properties of indocyanine green in human blood. *Invest Ophthalmol Vis Sci* 1998; 39: 1286–1290
- 23 Hagen A, Grosenick D, Macdonald R et al. Late-fluorescence mammography assesses tumor capillary permeability and differentiates malignant from benign lesions. *Opt Express* 2009; 17: 17016–17033
- 24 Alacam B, Yazici B, Intes X et al. Pharmacokinetic-rate images of indocyanine green for breast tumors using near-infrared optical methods. *Phys Med Biol* 2008; 53: 837–859
- 25 Schmitz CH, Klemer DP, Hardin R et al. Design and implementation of dynamic near-infrared optical tomographic imaging instrumentation for simultaneous dual-breast measurements. *Appl Opt* 2005; 44: 2140–2153
- 26 Barbour RL, Graber HL, Pei Y et al. Optical tomographic imaging of dynamic features of dense-scattering media. *J Opt Soc Am A Opt Image Sci Vis* 2001; 18: 3018–3036
- 27 Landsman ML, Kwang T, Mook GA et al. Light-absorbing properties, stability, and spectral stabilization of indocyanine green. *J Appl Physiol* 1976; 40: 575–583
- 28 Papadimitrou JM, Woods AE. Structural and functional characteristics of the microcirculation in neoplasms. *J Pathol* 1975; 116: 65–72
- 29 Weidner N, Semple JP, Welch WR et al. Tumor angiogenesis and metastasis – correlation in invasive breast carcinoma. *N Engl J Med* 1991; 324: 1–8
- 30 Tsutsui S, Kume M, Era S. Prognostic value of microvessel density in invasive ductal carcinoma of the breast. *Breast Cancer* 2003; 10: 312–319
- 31 Boetes C, Barentsz JO, Mus RD et al. MR characterization of suspicious breast lesions with a gadolinium-enhanced TurboFLASH subtraction technique. *Radiology* 1994; 193: 777–781
- 32 Dietzel M, Baltzer PA, Vag T et al. Potential of MR Mammography to Predict Tumor Grading of Invasive Breast Cancer. *Fortschr Röntgenstr* 2011; 183: 826–833 Epub 2011 Mar 25
- 33 Schnall MD, Blume J, Bluemke DA et al. Diagnostic architectural and dynamic features at breast MR imaging: multicenter study. *Radiology* 2006; 238: 42–53
- 34 Kuhl CK, Schild HH, Morakkabati N. Dynamic bilateral contrast-enhanced MR imaging of the breast: trade-off between spatial and temporal resolution. *Radiology* 2005; 236: 789–800
- 35 Schorn C, Fischer U, Luftner-Nagel S et al. Diagnostic potential of ultrafast contrast-enhanced MRI of the breast in hypervascularized lesions: are there advantages in comparison with standard dynamic MRI? *J Comput Assist Tomogr* 1999; 23: 118–122
- 36 Veltman J, Stoutjesdijk M, Mann R et al. Contrast-enhanced magnetic resonance imaging of the breast: the value of pharmacokinetic parameters derived from fast dynamic imaging during initial enhancement in classifying lesions. *Eur Radiol* 2008; 18: 1123–1133
- 37 Sardanelli F, Rescinito G, Giordano GD et al. MR dynamic enhancement of breast lesions: high temporal resolution during the first-minute versus eight-minute study. *J Comput Assist Tomogr* 2000; 24: 724–731
- 38 Cherrick GR, Stein SW, Leevy CM et al. Indocyanine green: observations on its physical properties, plasma decay, and hepatic extraction. *J Clin Invest* 1960; 39: 592–600
- 39 Poellinger A, Burock S, Grosenick D et al. Breast cancer: early- and late-fluorescence near-infrared imaging with indocyanine green – a preliminary study. *Radiology* 2011; 258: 409–416
- 40 Radjenovic A, Dall BJ, Ridgway JP et al. Measurement of pharmacokinetic parameters in histologically graded invasive breast tumours using dynamic contrast-enhanced MRI. *Br J Radiol* 2008; 81: 120–128
- 41 Huber S, Helbich T, Kettenbach J et al. Effects of a microbubble contrast agent on breast tumors: computer-assisted quantitative assessment with color Doppler US – early experience. *Radiology* 1998; 208: 485–489
- 42 Caproni N, Marchisio F, Pecchi A et al. Contrast-enhanced ultrasound in the characterisation of breast masses: utility of quantitative analysis in comparison with MRI. *Eur Radiol* 2010; 20: 1384–1395
- 43 Kettenbach J, Helbich TH, Huber S et al. Computer-assisted quantitative assessment of power Doppler US: effects of microbubble contrast agent in the differentiation of breast tumors. *Eur J Radiol* 2005; 53: 238–244

- 44 Kuhl CK, Traber F, Gieseke J et al. Whole-body high-field-strength (3.0-T) MR imaging in clinical practice. Part II. Technical considerations and clinical applications. *Radiology* 2008; 247: 16–35
- 45 Leff DR, Warren OJ, Enfield LC et al. Diffuse optical imaging of the healthy and diseased breast: a systematic review. *Breast Cancer Res Treat* 2008; 108: 9–22
- 46 Pfandzelter R, Wülfing U, Boedeker B et al. Die diagnostische Bildqualität von Mammografien in der vertragsärztlichen Versorgung Deutschlands. *Fortschr Röntgenstr* 2010; 182: 993–1000
- 47 Sommer A, Girnus R, Wendt B et al. Physikalisch-technische Qualitätssicherung im deutschen Mammografie-Screening-Programm: Erfahrungsbericht des Referenzzentrums Münster nach drei Jahren. *Fortschr Röntgenstr* 2009; 181: 447–453
- 48 Sommer A, Girnus R, Wendt B et al. Entwicklung eines objektiven Bewertungssystems für die jährliche physikalische Qualitätssicherung an digitalen Mammografie-Systemen. *Fortschr Röntgenstr* 2010; 182: 788–792
- 49 Sommer A, Lenzen H, Blaser D et al. Prüfanleitung für die Durchführung der ergänzenden Prüfpositionen nach EPQC 4th Edition für digitale Mammografie-Systeme Leitfaden der deutschen Referenzzentren für Mammografie: Version 1.4. *Fortschr Röntgenstr* 2009; 181: 845–850
- 50 Blendl C, Schreiber AC, Buhr H. Ergebnisse einer automatischen Auswertung von Prüfkörperaufnahmen nach PAS 1054 und IEC 62 220 – 1-2 an unterschiedlichen Typen digitaler Mammografie-Röntgeneinrichtungen. *Fortschr Röntgenstr* 2009; 181: 979–988
- 51 Weigel S, Batzler WU, Decker T et al. First Epidemiological Analysis of Breast Cancer Incidence and Tumor Characteristics after Implementation of Population-Based Digital Mammography Screening. *Fortschr Röntgenstr* 2009; 181: 1144–1150
- 52 Uhlenbrock DF, Mertelmeier T. Comparison of Anode/Filter Combinations in Digital Mammography with Respect to the Average Glandular Dose. *Fortschr Röntgenstr* 2009; 181: 249–254
- 53 Ketelsen D, Buchgeister M, Fenchel M et al. Estimation of Radiation Exposure of Prospectively Triggered 128-Slice Computed Tomography Coronary Angiography. *Fortschr Röntgenstr* 2010; 182: 1105–1109
- 54 Colin C, Devic C, Noël A et al. DNA double-strand breaks induced by mammographic screening procedures in human mammary epithelial cells. *Int J Radiat Biol* 29. Jul 2011
- 55 Jackman RJ, Marzoni Jr FA. Stereotactic histologic biopsy with patients prone: technical feasibility in 98% of mammographically detected lesions. *Am J Roentgenol* 2003; 180: 785–794